Journal of the Ceramic Society of Japan 132 [5] 227-231 2024
DOI https://doi.org/10.2109/jcersj2.23121

JCS-Japan

FULL PAPER

Effect of Si addition on epitaxial growth and gas sensing properties of tungsten oxide films

Yutaka Adachi[1,†]

[1] Affiliation Electro-ceramics Group, Research Center for Electronic and Optical Materials, National Institute for Materials Science (NIMS), 1–1 Namiki, Tsukuba, Ibaraki 305–0044, Japan

WO_3 epitaxial films with the same thickness and in-plane crystal grain size were prepared using pulsed laser deposition with various Si contents in the target to clarify the effect of Si addition to WO_3 on the gas sensing properties. X-ray diffraction measurements indicated that the films grown on the $(1\bar{1}02)$ face of sapphire had a (001) orientation with in-plane epitaxial relationships of $[110]WO_3//[01\bar{1}1]$ or $[110]WO_3//[2\bar{1}10]Al_2O_3$, regardless of the Si content. Scanning probe microscopy observations revealed that particles with a diameter of several tens of nanometers grow on the surface of the Si-doped WO_3 film. Measurements of the gas response to ethanol and acetone showed superior gas selectivity towards acetone gas at low temperatures, which is due to the catalytic effect of SiO_x particles on the film surface.

Key-words : Tungsten trioxide, Epitaxial film, Si doping, Acetone, Ethanol, Gas selectivity

[Received June 23, 2023; Accepted February 25, 2024]

1. Introduction

N-type oxide semiconductors such as zinc oxide and tin oxide have been studied for application as gas sensors and are already in practical use.[1)] Oxide semiconductor gas sensors have advantages such as relatively high sensitivity, ease of miniaturization, and relatively low cost, which makes them suitable for use in mobile devices and sensor network applications; however, they have the disadvantage of poor gas selectivity.[2)] This drawback must be addressed for applications such as health monitoring devices that would allow users to easily check their health at home by breath analysis, and sensor networks that would monitor air pollution gases such as SO_x and NO_x.

Gas detection with oxide semiconductor gas sensors uses the change in the electrical resistance of the semiconductor caused by the reaction between oxygen adsorbed on the sensor surface and the target gas to be detected, such as hydrogen or ethanol. Therefore, similar reducing gases in the atmosphere cause similar changes in the electrical resistance of the sensor, and this is one of the reasons for the poor gas selectivity of oxide semiconductor gas sensors. As such, there have been many attempts to increase the response to only specific gases by the addition of impurities.[3)–5)]

Tungsten oxide (WO_3) is also known as a matrix material for oxide semiconductor gas sensors, and it has been reported to respond to NO_x,[6)–9)] O_2,[10)–12)] H_2S,[13)–15)] and volatile organic compound gases[16),17)] when doped with various impurities. However, the role of impurity doping on the improvement of gas selectivity has yet to be clarified, especially with respect to the selection of additive impurity species to increase the response to a particular gas.

The reason why the effect of impurity addition is unclear is probably because the sensor characteristics are affected not only by the addition of impurities, but also by changes such as the particle size, shape, and the crystal facet exposed on sensor surfaces.[18)–24)] Oxide powders or nanostructures are typically employed for semiconductor gas sensors. In the case of powders and nanostructures, the addition of impurities to improve sensor performance tends to change other parameters such as the shape and size of the sensor matrix particles.[25)] It is important to correlate material parameters such as the grain size and shape to obtain clear guidelines for improvement of the gas sensing properties. Therefore, to elucidate the true effect of impurity addition, it is necessary to prepare and compare samples in which only the impurity addition concentration differs, while other parameters, such as the particle size and shape, are the same.

In this study, we have attempted to use epitaxial thin films as gas sensors to clearly capture the effect of impurity addition. The thickness of epitaxial films can be easily controlled, and it is possible to fabricate samples with uniform particle sizes. In addition, only specific crystal planes of these thin films are exposed on the topmost surface; therefore, the influence of differences in the crystal planes on the sensor properties can be suppressed. Furthermore, the same in-plane crystal orientation can be produced; therefore, the influence of the bonding state between crystal grains can be expected to be suppressed. The author has successfully clarified the effects of spontaneous polarization and Mg addition on the gas sensing properties of zinc

† Corresponding author: Y. Adachi; E-mail: adachi.yutaka@nims.go.jp

oxide (ZnO) epitaxial thin films used as gas sensors.[23),24)] In this study, epitaxial WO_3 thin films doped with Si were prepared on sapphire substrates to investigate how the sensor properties depend on the Si concentration. Sensors that exhibit excellent gas selectivity for acetone are required for the development of hand-held breath analysis instruments. Righettoni et al. reported that Si-doped WO_3 exhibits excellent acetone gas selectivity;[26)] however, the mechanism that underlies this effect is still unclear. Clarification of the mechanism for the effect of Si addition is thus expected to contribute to further improvement of acetone gas sensing selectivity.

2. Experimental details

Si-doped WO_3 films were prepared by pulsed laser deposition using a KrF excimer laser ($\lambda = 246$ nm) with a pulse width of 20 ns, a repetition rate of 5 Hz, and a laser fluence of approximately 1 J/cm^2. The background pressure in the growth chamber was less than 4×10^{-7} Pa. Si-doped WO_3 ceramics (Toshima Co. Ltd.) were used as a target. The films were grown at oxygen (O_2) pressures of 1.3×10^{-3} to 33.3 Pa, at substrate temperatures (T_g) in the range of 350–650 °C. The films were deposited on the $(10\bar{1}2)$ face of sapphire to obtain epitaxial films.

The film thickness was determined by X-ray reflectivity (PANalytical X'Pert MRD) measurements with Cu Kα radiation. The orientation and crystallinity of the films were determined by X-ray diffraction analysis (XRD; PANalytical X'Pert MRD, Cu Kα radiation and a hybrid monochromator consisting of a coupled X-ray mirror and a 2-bounce Ge 220 monochromator). The film morphology was investigated with tapping mode scanning probe microscopy (SPM; SII SPA-400). An in-house-built gas sensing test system was used to measure the gas sensing properties of the Si-doped WO_3 films. The details of this test system have been described elsewhere.[22)] The gas response to synthetic air and the target gas (40 ppm H_2, ethanol, acetone) were measured at operating temperatures of 150–350 °C. The working voltage of the measurement circuit was set to 1 V and the film resistance was measured. The sensor response S, was determined via

$$S = R_a/R_g \quad (1)$$

where R_a and R_g are the sample resistances in synthetic air and the target gas, respectively.

3. Results and discussion

The effect of the oxygen partial pressure introduced during film deposition was investigated to determine the growth conditions for epitaxial films. **Figure 1** shows XRD measurement results for films fabricated at various oxygen partial pressures in the range from 1.3×10^{-3} to 33.3 Pa. When the oxygen partial pressure was as low as 1.3×10^{-3} Pa, only a diffraction peak due to WO_2 was observed, and no diffraction peaks associated with WO_3 appeared. When the oxygen partial pressure was increased to 5.6 Pa, diffraction peaks due to WO_3 002 and 004 began to appear. When the oxygen partial pressure was further

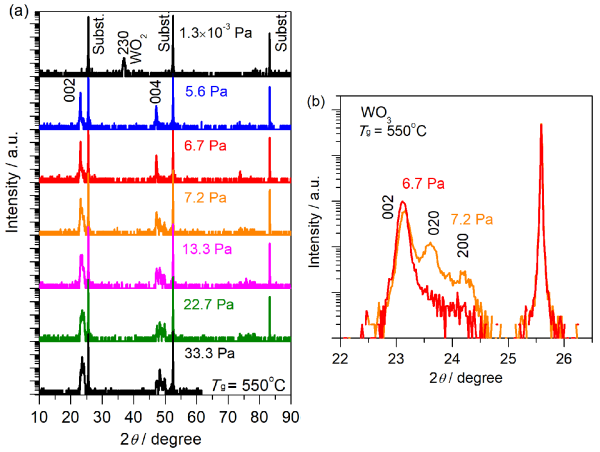

Fig. 1. (a) XRD profiles for WO_3 films grown on r-plane sapphire substrates at oxygen partial pressures in the range from 1.3×10^{-3} to 33.3 Pa. (b) Magnified view of the 2θ range from 22.0 to 26.5 degrees.

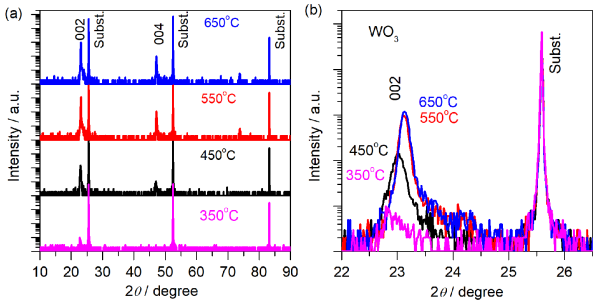

Fig. 2. (a) XRD profiles for WO_3 films grown on r-plane sapphire substrates at temperatures in the range from 350 to 650 °C. (b) Magnified view of the 2θ range from 22.0 to 26.5 degrees.

increased, two more peaks appeared near the 002 and 004 diffraction peaks. Figure 1(b) shows a magnified view of the 2θ range from 22.0 to 26.5 degrees, and these peaks can be indexed as 020 and 200 diffractions from monoclinic WO_3. These results indicate that when the oxygen partial pressure is low during film growth, WO_3 does not grow because the oxygen supply is insufficient, and instead, the growth of oxygen-deficient WO_2 occurs. When oxygen is supplied at around 5.6 Pa, (001) oriented WO_3 films are then grown. If the oxygen partial pressure is further increased, then polycrystalline films with (100) and (010) oriented crystal grains are formed.

Next, the temperature for epitaxial growth was optimized. **Figure 2** shows the XRD measurement results for films fabricated at various growth temperatures while the oxygen partial pressure was kept constant at 6.7 Pa. The intensity of the diffraction peaks associated with WO_3 became weaker as the growth temperature decreased, and the 002 diffraction peak tended to shift toward lower angles, as shown in Fig. 2(b). This is due to a decrease in crystallinity and the formation of defects in the films. Therefore, this result indicates that film growth at temperatures higher than 550 °C is necessary to grow films with the desired degree of crystallinity.

Table 1. Structural information for the WO_3 phases[27)]

Structure	Symbol	Space group	Lattice parameters
Monoclinic	γ	$P2_1/n$	$a = 0.7301$ nm $b = 0.7538$ nm $c = 0.7689$ nm $\beta = 90.893°$
Tetragonal	α	$Pmnb$	$a = 0.5250$ nm $c = 0.3915$ nm

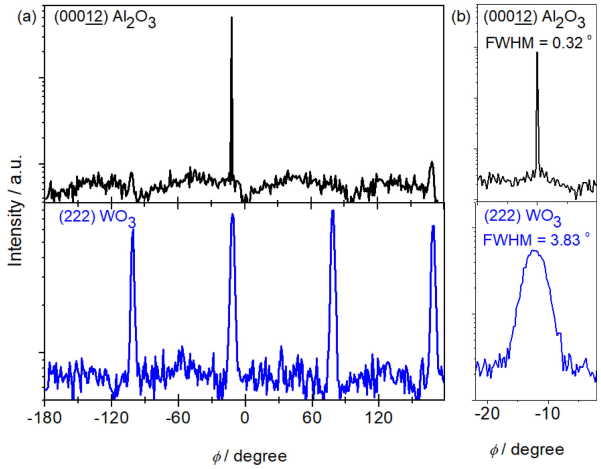

Fig. 3. (a) φ scans of the WO_3 222 diffraction peaks for undoped WO_3 film. A φ scan of the Al_2O_3 00012 diffraction peak is also shown as a reference. (b) Magnified view of the Al_2O_3 00012 and WO_3 222 diffraction peaks.

To determine the in-plane orientation of the prepared films, φ scans of the WO_3 222 diffraction peaks were performed. **Table 1** shows the space groups and lattice constants of monoclinic and tetragonal WO_3. Only four diffraction peaks were observed in **Fig. 3**, which indicates that the films have 4-fold symmetry and that tetragonal crystals were grown. However, tetragonal WO_3 is a high-temperature phase observed above 720 °C; therefore, it is unlikely that tetragonal crystals were formed. Monoclinic WO_3 is stable at room temperature; therefore, there is a high possibility that monoclinic crystal was formed. However, if a monoclinic WO_3 film was formed, then only two diffraction peaks should be observed in the 222 φ scan due to the symmetry of a (001) oriented monoclinic WO_3 film. The reason why four diffraction peaks were observed could be that (001) oriented monoclinic WO_3 grew with in-plane 90-degree rotational domains. The full width at half maximum (FWHM) of the WO_3 222 diffraction peak for undoped WO_3 was unnaturally broad at 3.83 degrees. The reason for this unnaturally broad FWHM is that the 222 and $2\bar{2}2$ diffraction peaks, which should be separately observed due to the rectangular ab-plane, were overlapped due to the insufficient crystallinity of the film. Only four peaks were observed in the φ scan, which indicates there were no 45-degree rotational domains, and the in-plane orientation of the film is the substrate $[10\bar{1}1]$ direction and the $\langle 110 \rangle$ direction for WO_3 are parallel to each other. These results indicate that (001) oriented epitaxial WO_3 films with 90-degree in-plane rotation domains can be grown at an oxygen pressure of around 6.7 Pa and a temperature of 550 °C.

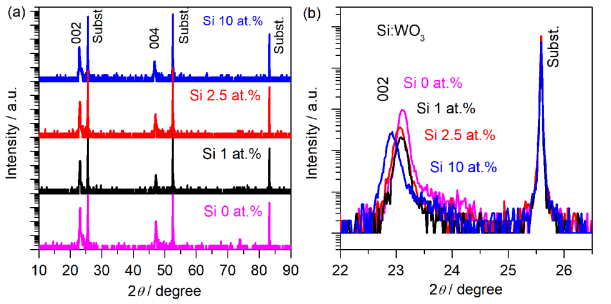

Fig. 4. (a) XRD profiles for Si-doped WO_3 films grown on r-plane sapphire substrates at Si concentrations in the range from 0 to 10 at %. (b) Magnified view of the 2θ range from 22.0 to 26.5 degrees.

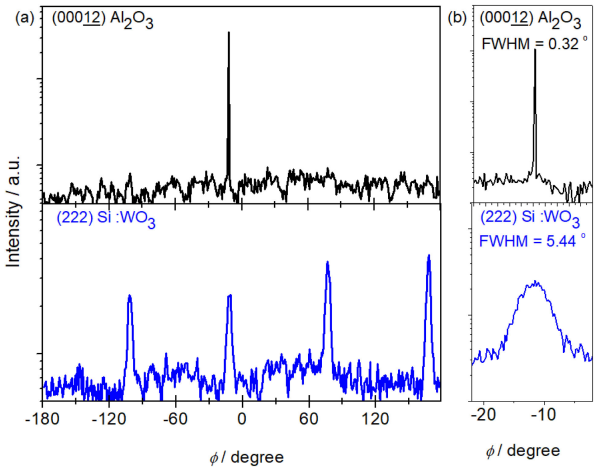

Fig. 5. (a) φ scans of the WO_3 222 diffraction peaks for Si 10 at.% doped WO_3 film. A φ scan of the Al_2O_3 00012 diffraction peak is also shown as a reference. (b) Magnified view of the Al_2O_3 00012 and WO_3 222 diffraction peaks.

Films were prepared using Si-doped WO_3 targets under the described growth conditions. **Figure 4** shows the XRD results for the prepared films. All the films prepared from the 1, 2.5 and 10 % Si-doped targets showed (001) orientation. Figure 4(b) shows an enlarged view in the vicinity of the 002 diffraction peak; the 002 peak tends to shift toward lower angles as the Si content increases. This may be due to the presence of Si in the crystal lattice or the formation of crystal defects in the films.

Figure 5 shows φ scan measurement results for the WO_3 film prepared with the 10 % Si-doped target. As with the undoped WO_3 film only four diffraction peaks were observed, which indicates that the in-plane orientation of the film is the same as that of the undoped film and the Si-doped films also have 90-degree in-plane rotation domains.

Epitaxial films were obtained for both the undoped WO_3 and Si-doped WO_3 targets, and the gas sensing properties of these films were measured. **Table 2** gives the thicknesses of these films. The gas sensing response of the undoped WO_3 and 1 % Si doped films are shown in **Figs. 6**(a) and 6(b). Two points should be noted regarding

Table 2. Thickness of undoped and Si-doped WO_3 films used in this study

Sample	Film thickness [nm]
Undoped WO_3	25
1 at.% Si-doped WO_3	34
2.5 at.% Si-doped WO_3	23
10 at.% Si-doped WO_3	22

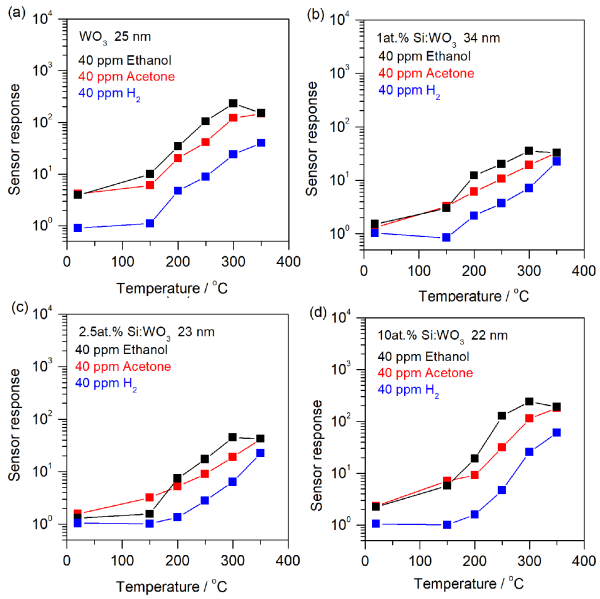

Fig. 6. Temperature-dependent sensor response to 40 ppm H_2, acetone and ethanol for (a) 0 at.%, (b) 1 at.%, (c) 2.5 at.%, and (d) 10 at.% Si-doped WO_3 films.

these measurements. First, the responses for acetone and ethanol are almost the same at 350 °C. The maximum response for ethanol occurs around 300 °C, while that for acetone is larger and occurs above 350 °C. Measurements were made only up to 350 °C to prevent degradation of the gold electrode fabricated on the film surface. However, it is expected that measurements at higher temperatures would show a higher response for acetone than for ethanol. The other point is that the response in the range of 200 to 300 °C tended to increase in the order of ethanol > acetone > hydrogen, although the response of the Si-doped sample toward ethanol at 150 °C was almost the same as that for acetone.

As the Si concentration was further increased, the response toward acetone at 150 °C exceeded that of ethanol. Figures 6(c) and 6(d) show the results of WO_3 sensing measurements with the addition of 2.5 % and 10 % Si, respectively. The addition of 10 % Si reduced the difference between the responses toward acetone and ethanol, although the response toward acetone still exceeded that for ethanol. This trend was not observed for the undoped WO_3 film, which suggests that this is due to Si addition. On the other hand, the behavior at high temperatures showed the same trend as that without Si addition and with 1 % Si addition; therefore, this response could be tungsten oxide-derived rather than an effect of Si addition.

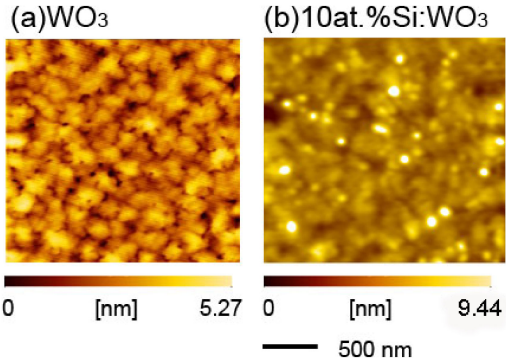

Fig. 7. SPM images of (a) WO_3 and (b) 10 at.% Si-doped WO_3 films grown on r-plane sapphire substrates.

The reason for these changes in the sensor properties is as follows. There are two different effects that improve sensor properties through impurity doping or addition: electrical and chemical sensitization effects.[28] One is the effect of a residual electron concentration. If the reaction shown in Eq. (2) occurs on the surface of the sensor, then the presence or absence of the target gas will cause a change in the electron concentration in the film.

$$O_{\mathrm{ads}} + X \rightarrow XO + 2e^{-}. \quad (2)$$

Assuming that the change of the electron concentration in the film due to the absorption and desorption of oxygen on the surface is $\delta\sigma$ and that the electron mobility μ does not change by the atmospheric gas, the sensor response S is expressed as:

$$S = \frac{R_{\mathrm{a}}}{R_{\mathrm{g}}} = \frac{\sigma_{\mathrm{n\_g}}}{\sigma_{\mathrm{n\_air}}} = \frac{\sigma_{\mathrm{n\_air}} + \delta\sigma_{\mathrm{n}}}{\sigma_{\mathrm{n\_air}}} = 1 + \frac{\delta\sigma_{\mathrm{n}}}{\sigma_{\mathrm{n\_air}}}, \quad (3)$$

where R_{a} and R_{g} are the sensor resistance in air and in the target gas, respectively. $\sigma_{\mathrm{n\_g}}$ and $\sigma_{\mathrm{n\_air}}$ are the electron concentrations in the film when exposed to the target gas and air, respectively. If the concentration of the target gas is constant, i.e., $\delta\sigma_{\mathrm{n}}$ is constant, then this equation indicates that a smaller residual electron concentration in air, i.e., a larger resistance value, will give a larger sensor response. However, this equation does not explain the difference in the response with respect to the gas type.

Another mechanism to improve the sensor response properties is the chemical sensitization effect. This is an effect in which impurities on the surface of the semiconductor sensor matrix promote adsorption and dissociation of the target gas and enhance the reaction of adsorbed gas with adsorbed oxygen. As shown in **Fig. 7**, SPM observations indicated Si or SiO_x particles with a diameter of approximately several tens nm on the top surface of the films prepared with the Si-doped target; therefore, these particles may have enhanced the response to acetone at 150 °C.

A shift in the maximum response at high temperatures was observed for all the thin films prepared in this study. It is assumed that there are many acetone adsorption sites that involve W atoms on the film surface. A maximum response shift at high temperature was observed for all the sensors

regardless of whether Si was doped or not. Therefore, the amount of doped Si has no relation to the maximum response temperature shift. In the case of MgZnO film sensors, the maximum response to acetone is at approximately 300 °C.[24] On the other hand, that for the WO_3 films is over 350 °C, which indicates that the maximum response temperature shift for WO_3 films due to the characteristics of the adsorption sites that involve W atoms.

The temperature dependence of the sensor response values is determined by the chemical reaction rate at adsorption sites at a certain temperature. If the catalytic effect of Si on the sensor response is not significant at high temperatures, then the temperature dependence of the response value is determined by the chemical reaction rate at the adsorption sites and is not affected by the number of adsorption sites. As the Si concentration increases, the number of adsorption sites decreases; therefore, the response value at each temperature should decrease as the Si addition concentration increases. However, if the number of adsorption sites on the surface is sufficiently greater than the number of acetone gas molecules present on the surface of the sensor body under equilibrium conditions at a certain temperature, then the sensor response value will not be affected by the Si dopant concentration but will be affected by the characteristic of the adsorption sites that involve W atoms. Therefore, the sensor response characteristics at high temperatures are be determined by the chemical reaction rate of adsorption sites that involve W atoms present on the thin film surface, and the catalytic action of Si or SiO_x has no significant influence.

4. Conclusion

Epitaxial WO_3 films were fabricated without any variation in particle size, shape and inter-particle bonding state, but with differing Si concentrations to clarify the effect of Si addition to WO_3. All of the samples prepared in this study showed the highest response to ethanol at 300 °C regardless of the Si content, but the highest response to acetone was observed at 350 °C. This result indicates that tungsten atoms on the surface result in a shift of the maximum sensing response temperature. On the other hand, the addition of Si resulted in a larger response to acetone than to ethanol at 150 °C or lower. Particles of several tens nm in diameter were observed on the surface of the Si-doped WO_3 films; therefore, the improvement of the acetone response at low temperatures is due to the catalytic effect of these particles. The results of this study are expected to contribute to the development for sensors with excellent gas selectivity.

Acknowledgments This work was partly supported by a Kakenhi Grant-in-Aid (No. 21K04647) from the Japan Society for the Promotion of Science (JSPS).

References

1) H. Ji, W. Zeng and Y. Li, *Nanoscale*, **11**, 22664–22684 (2019).
2) Q. Ren, Y.-Q. Cao, D. Arulraj, C. Liu, D. Wu, W.-M. Li and A.-D. Li, *J. Electrochem. Soc.*, **167**, 067528 (2020).
3) K. Vijayalakshmi and A. Renitta, *Ceram. Int.*, **41**, 14315–14325 (2015).
4) A. S. M. I. Uddin and G. S. Chung, *Sensor. Actuat. B-Chem.*, **231**, 601–608 (2016).
5) F. Fan, J. Zhang, J. Li, N. Zhang, R. R. Hong, X. Deng, P. Tang and D. Li, *Sensor. Actuat. B-Chem.*, **241**, 895–903 (2017).
6) E. Rossinyol, A. Prim, E. Pellicer, J. Rodríguez, F. Peiró, A. Cornet, J. R. Morante, B. Tian, T. Bo and D. Zhao, *Sensor. Actuat. B-Chem.*, **126**, 18–23 (2007).
7) M. Penza, C. Martucci and G. Cassano, *Sensor. Actuat. B-Chem.*, **50**, 52–59 (1998).
8) M. Akiyama, J. Tamaki, N. Miura and N. Yamazoe, *Chem. Lett.*, **9**, 1611–1614 (1991).
9) P. Ivanov, E. Llobet, F. Blanco, A. Vergara, X. Vilanova, I. Gracia, C. Cané and X. Correig, *Sensor. Actuat. B-Chem.*, **118**, 311–317 (2006).
10) M. Gillet, K. Aguir, M. Bendahan and P. Mennini, *Thin Solid Films*, **484**, 358–363 (2005).
11) A. Labidi, E. Gillet, R. Delamare, M. Maaref and K. Aguir, *Sensor. Actuat. B-Chem.*, **120**, 338–345 (2006).
12) S. Vallejos, V. Khatko, K. Aguir, K. A. Ngo, J. Calderer, I. Gràcia, C. Cané, E. Llobet and X. Correig, *Sensor. Actuat. B-Chem.*, **126**, 573–578 (2007).
13) A. Ponzoni, E. Comini, G. Sberveglieri, J. Zhou, S. Z. Deng, N. S. Xu, Y. Ding and Z. L. Wang, *Appl. Phys. Lett.*, **88**, 203101 (2006).
14) R. Ionescu, A. Hoel, C. G. Granqvist, E. Llobet and P. Heszler, *Sensor. Actuat. B-Chem.*, **104**, 132–139 (2005).
15) C. S. Rout, M. Hegde and C. N. R. Rao, *Sensor. Actuat. B-Chem.*, **128**, 488–493 (2008).
16) K. Kanda and T. Maekawa, *Sensor. Actuat. B-Chem.*, **108**, 97–101 (2005).
17) J. Hubálek, K. Malysz, J. Prášek, X. Vilanova, P. Ivanov, E. Llobet, J. Brezmes, X. Correig and Z. Svěrák, *Sensor. Actuat. B-Chem.*, **101**, 277–283 (2004).
18) G. K. Mani and J. B. B. Rayappan, *Appl. Surf. Sci.*, **311**, 405–417 (2014).
19) S. Ilican, M. Caglar and Y. Caglar, *Appl. Surf. Sci.*, **256**, 7204–7210 (2010).
20) G. Korotcenkov, *Mat. Sci. Eng. B-Solid*, **139**, 1–23 (2007).
21) S. Fukami, M. Taguchi, Y. Adachi, I. Sakaguchi, K. Watanabe, T. Kinoshita, T. Muro, T. Matsushita, F. Matsui, H. Daimon and T. T. Suzuki, *Phys. Rev. Appl.*, **7**, 064029 (2017).
22) Y. Adachi, K. Watanabe, N. Saito, I. Sakaguchi and T. T. Suzuki, *J. Ceram. Soc. Jpn.*, **124**, 668–672 (2016).
23) Y. Adachi, N. Saito, I. Sakaguchi and T. T. Suzuki, *Thin Solid Films*, **685**, 238–244 (2019).
24) Y. Adachi, *Surf. Interfaces*, **28**, 101597 (2022).
25) S. Mridha and D. Basak, *J. Phys. D Appl. Phys.*, **40**, 6902–6907 (2007).
26) M. Righettoni, A. Tricoli and S. E. Pratsinis, *Chem. Mater.*, **22**, 3152–3157 (2010).
27) P. M. Woodward, A. W. Sleight and T. Vogt, *Solid State Chem.*, **131**, 9–17 (1997).
28) A. Šutka and K. A. Gross, *Sensor. Actuat. B-Chem.*, **222**, 95–105 (2016).